JACS
JOURNAL OF THE AMERICAN CHEMICAL SOCIETY

Communication

pubs.acs.org/JACS

Understanding the Cubic Phase Stabilization and Crystallization Kinetics in Mixed Cations and Halides Perovskite Single Crystals

Li-Qiang Xie,[†] Liang Chen,[†] Zi-Ang Nan, Hai-Xin Lin, Tan Wang, Dong-Ping Zhan, Jia-Wei Yan, Bing-Wei Mao,[*] and Zhong-Qun Tian

State Key Laboratory of Physical Chemistry of Solid Surfaces, Department of Chemistry, College of Chemistry and Chemical Engineering, iChEM, Xiamen University, Xiamen 361005, China

Supporting Information

ABSTRACT: The spontaneous α-to-δ phase transition of the formamidinium-based (FA) lead halide perovskite hinders its large scale application in solar cells. Though this phase transition can be inhibited by alloying with methylammonium-based (MA) perovskite, the underlying mechanism is largely unexplored. In this Communication, we grow high-quality mixed cations and halides perovskite single crystals $(FAPbI_3)_{1-x}(MAPbBr_3)_x$ to understand the principles for maintaining pure perovskite phase, which is essential to device optimization. We demonstrate that the best composition for a perfect α-phase perovskite without segregation is $x = 0.1-0.15$, and such a mixed perovskite exhibits carrier lifetime as long as 11.0 μs, which is over 20 times of that of $FAPbI_3$ single crystal. Powder XRD, single crystal XRD and FT-IR results reveal that the incorporation of MA^+ is critical for tuning the effective Goldschmidt tolerance factor toward the ideal value of 1 and lowering the Gibbs free energy via unit cell contraction and cation disorder. Moreover, we find that Br incorporation can effectively control the perovskite crystallization kinetics and reduce defect density to acquire high-quality single crystals with significant inhibition of δ-phase. These findings benefit the understanding of α-phase stabilization behavior, and have led to fabrication of perovskite solar cells with highest efficiency of 19.9% via solvent management.

Organic–inorganic lead halide perovskites have emerged as a class of promising materials for low-cost solution processing solar cells with power conversion efficiency (PCE) increased dramatically from 3.8% to 22.1% since 2009.[1−7] This material, with the formula ABX_3 (A = Cs, methylammonium (MA), formamidinium (FA); B = Pb, Sn; X = I, Br, Cl), provides a variety of opportunities to tune photovoltaic properties through facile compositional engineering and alloying.[6,8−11] Compared with $MAPbI_3$, replacing A site with FA can reduce the bandgap from 1.51 to 1.40 eV,[12,13] which is closer to the best 1.34 eV value as predicted by the Shockley–Queisser limit and better matches the solar spectrum.[3,14] In addition, $FAPbI_3$ demonstrates better thermal stability than $MAPbI_3$ due to stronger interactions within the perovskite.[15] This makes $FAPbI_3$ most likely the champion material for perovskite solar cells that have recently attracted more and more research interest. However, $FAPbI_3$ suffers from the well-known spontaneous phase transition from the desired α-phase black perovskite to δ-phase yellow nonperovskite at room temperature.[8,14,15] This phase transition is the main obstacle for high efficiency and long-term stability of $FAPbI_3$-based perovskite solar cells.

Fortunately, the undesired α-to-δ phase transition of FA-based perovskites can be largely inhibited through cation incorporation.[8,14,16−18] To date, the reported best cells are fabricated using the mixed cations perovskites because of their outstanding stability under illumination, humidity and thermal stress.[14,16−19] Investigations of the underlying mechanism of α-phase stabilization are essential for further improving the cell performance. Zhu et al.[20,21] reported the incorporation of cations with smaller effective radius can adjust the Goldschmidt tolerance factor or relax the crystal strain of FA-based perovskites. Meanwhile, others reported the larger entropy induced by cation disorder at high temperature plays crucial roles on α-phase stabilization.[17,22] However, most of the reported works are based on polycrystalline films, which are prepared mostly by spin-coating and contain rich amount of grain boundaries and defects. As a matter of fact, the spin-coating process introduces a number of kinetic factors such as temperature, atmosphere, humidity and antisolvent effect, which complicate the crystallization process[23] and affect the quality of perovskite films. Even though the stability of $FAPbI_3$ is greatly increased in the form of single crystal, the α-to-δ phase transition still exists.[24]

Herein, we report rapid growth of high-quality single crystals of mixed cations and halides perovskite, with the formula $(FAPbI_3)_{1-x}(MAPbBr_3)_x$, and investigate the thermodynamic and kinetic effects of MA^+ and Br^- incorporation on the α-phase stabilization of the mixed cations and halides perovskite and thus provide guidance for device optimization.

The growth of centimeter sized single crystals of $(FAPbI_3)_{1-x}(MAPbBr_3)_x$ ($x = 0$, 0.05, 0.1, 0.15, 0.2) is achieved based on inverse temperature crystallization (ITC) method.[12,25,26] Figure 1 provides a schematic illustration of the crystal growth process with a photograph of a typical crystal with size reaching 15 mm. In this process, small crystal seeds, grown in the 100 °C precursor solution, are placed in a fresh 1 M precursor solution for growth of large crystals (see experimental details in Supporting Information). Perovskite single crystals with varying x bear similar rhombic dodecahedra geometry as shown in Figure S1, demonstrating that the ITC method can be successfully

Received: December 2, 2016
Published: February 17, 2017

DOI: 10.1021/jacs.6b12432
J. Am. Chem. Soc. 2017, 139, 3320−3323

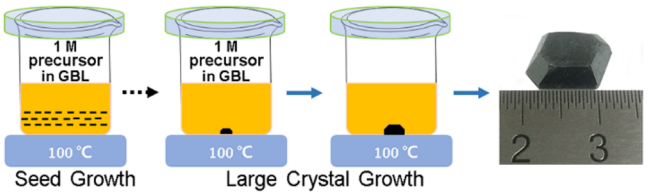

Figure 1. Schematic illustration of crystal growth process.

applied to grow high-quality mixed cations and halides perovskite single crystals.

A series of characterizations are performed to prove that $MAPbBr_3$ has been alloyed with $FAPbI_3$ and to study the properties of $(FAPbI_3)_{1-x}(MAPbBr_3)_x$ ($x = 0, 0.05, 0.1, 0.15, 0.2$) single crystals. UV−vis−NIR spectral results demonstrate that the absorption onset of $FAPbI_3$ single crystal locates at about 890 nm. The absorption edge and the steady state photoluminescence (PL) peak both shift to low wavelength when x increases from 0 to 0.20, which indicates the $MAPbBr_3$ has been successfully alloyed with $FAPbI_3$, as shown in Figure 2A,B. In the

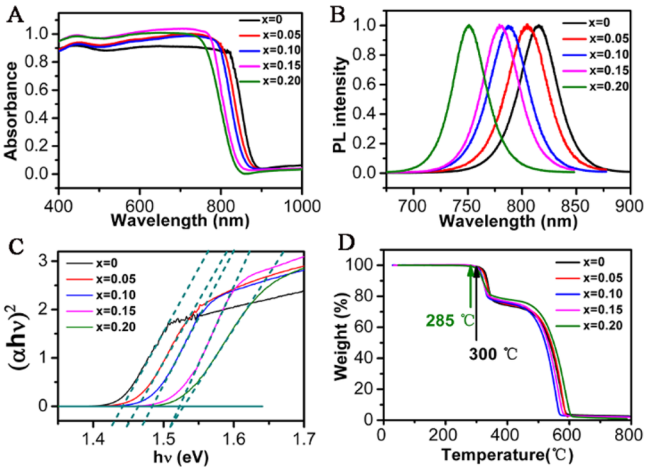

Figure 2. (A) UV−vis−NIR absorption spectra, (B) steady-state photoluminescence spectra, (C) Tauc Plot and (D) TGA of mixed cations and halides perovskite single crystals $(FAP\text{-}bI3)_{1-x}(MAPbBr_3)x$ with $x = 0$, 0.05, 0.10, 0.15 and 0.20.

FT-IR spectrum of the $x = 0.15$ sample, vibrations of both MA^+ and FA^+ are observed, confirming again the alloying in the single crystal (see the detail analysis in Figure S2). Furthermore, the bandgap of $(FAPbI_3)_{1-x}(MAPbBr_3)_x$ single crystals can be deduced from Tauc plot (Figure 2C), which is valuable for optimization of device structure and materials. The bandgap is 1.43, 1.46, 1.48, 1.52 and 1.53 eV for $x = 0$, 0.05, 0.10, 0.15 and 0.20, respectively. We note that, when x reaches 0.20, the slope of the absorption edge decreases dramatically and PL peak undergoes remarkable blue-shift, which indicates different optical property from those of other compositions. The thermal stability of the mixed cations and halides perovskites is also studied using thermal gravity analysis (TGA), and the results are shown in Figure 2D. When x increases from 0 to 0.20, the decomposition temperature of these perovskites in N_2 atmosphere slightly decreases from 300 to 285 °C, the latter being still higher than that of $MAPbI_3$ single crystal (240 °C).[15] The details of each weight loss process are described in Figure S3.

To study the phase composition of FA-based perovskite crystals, XRD measurements are performed for powders ground from single crystals. $FAPbI_3$ undergoes spontaneous phase transition from the desired black perovskite phase (α-phase) to the undesired yellow nonperovskite phase (δ-phase) at room temperature, which induces serious cell performance drop. However, XRD results in Figure 3A show that the peak of δ-

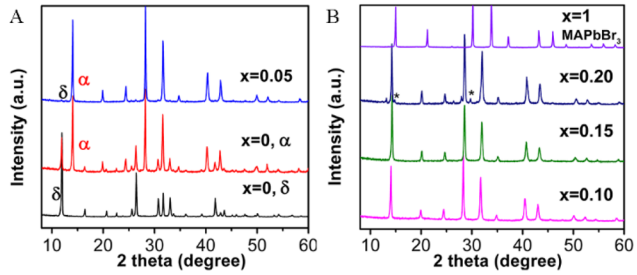

Figure 3. XRD patterns of perovskite single crystals after being stored overnight in argon filled glovebox: (A) yellow δ-$FAPbI_3$, α-$FAPbI_3$ after partial phase transition and $(FAP\text{-}bI_3)_{1-x}(MAPbBr_3)x$, with $x = 0.05$; (B) $(FAPbI_3)_{1-x}(MAPbBr_3)_x$, with $x = 0.10$, 0.15, 0.20 and 1.

phase has been largely inhibited in single crystalline $(FAP\text{-}bI_3)_{0.95}(MAPbBr_3)_{0.05}$, though a small peak is seen in the enlarged pattern (see Figure S4). When x increases to 0.10 and 0.15, all peaks can be assigned to arise from α-phase perovskite, which means full inhibition of the δ-phase, see Figure 3B. But in the case of $x = 0.20$, there appears weak peaks that are assigned to $MAPbBr_3$, indicating that phase segregation will occur with a large $MAPbBr_3/FAPbI_3$ ratio. We also observed that the corresponding perovskite turns to brown in the bulk after weeks of aging. This phase segregation may account for the observed unusual optical property mentioned above. These results reveal that the best composition for mixed cations and halides single crystals is $x = 0.10$ to 0.15, and such crystals are very stable in glovebox even after 6 months of storage. Next, we will focus on the crystals with $x = 0.15$, that is $(FAP\text{-}bI_3)_{0.85}(MAPbBr_3)_{0.15}$, for further analysis.

To understand further the effect of $MAPbBr_3$ alloying on α-phase stabilization, single crystal XRD measurements are performed to study the structure of $(FAPbI_3)_{0.85}(MAPbBr_3)_{0.15}$, and the results are shown in Figure 4. The unit cell shows a cubic structure ($Pm\bar{3}m$ (221) space group) with $a = b = c = 0.6224$ nm and cell volume of 241.13 Å^3. The predicted powder XRD pattern perfectly matches the experimentally measured one

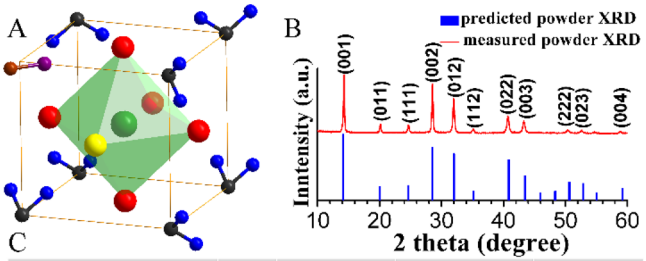

	Phase	Space-group	Cell Parameters	Cell Volume
$(FAPbI_3)_{0.85}(MAPbBr_3)_{0.15}$	cubic	Pm-3m(221)	a=b=c=6.224 Å	241.13 Å^3
[1]$FAPbI_3$	cubic	Pm3m	a=b=c=6.362 Å	257.51 Å^3

Figure 4. (A) Crystal structure (black, carbon; blue, nitrogen; green, lead; red, iodine; yellow, bromine and the carbon of MA, brown; nitrogen, violet); (B) predicted and experimental measured powder XRD patterns; (C) cell parameters of $(FAPbI_3)_{0.85}(MAPbBr_3)_{0.15}$ and $FAPbI_3$.[27]

DOI: 10.1021/jacs.6b12432
J. Am. Chem. Soc. 2017, 139, 3320−3323

where all peaks can be indexed to a cubic perovskite. Comparing the unit cell parameters of $(FAPbI_3)_{0.85}(MAPbBr_3)_{0.15}$ with that of cubic $FAPbI_3$,[27] we found that the unit cell contracts from 257.51 to 241.13 Å^3. Powder XRD results also support the cell contraction by the fact that the 001, 002 and 012 peaks shift toward higher angles as x increases, and the contraction becomes strongest at $x = 0.15$ (Figure S5). The peak shifting toward higher angle indicates a decrease in lattice parameter, which is consistent with the single crystal XRD results. The lattice contraction is probably due to the incorporation of much smaller MA^+ (ionic radius 217 pm) compared with that of FA^+ (253 pm),[28] which results in reduction of octahedral volume for the A-site cation surrounded by PbX_3^- octahedron in the unit cell. This cell contraction adjusts the effective Goldschmidt tolerance factor[28] toward 1, favorable to stabilize the cubic perovskite. On the other hand, incorporation of MA^+, which is of stronger dipole and more flexible rotation, may enhance the contribution of entropy due to higher degree of cation disorder as revealed by the crystal structure (Figure S6).[29] These results confirm that the incorporation of MA^+ plays important roles in stabilizing the black perovskite phase from thermodynamics point of view.

The mixed halides also play important roles in cubic phase stabilization, but from kinetics point of view. To investigate the effect from Br incorporation, we prepared the $(FAPbI_3)_{0.85}(MAPbI_3)_{0.15}$ single crystal using the same method. Surprisingly, the XRD results indicate insufficient inhibition of δ-phase, as shown in Figure 5A. The peak intensity of δ-phase is

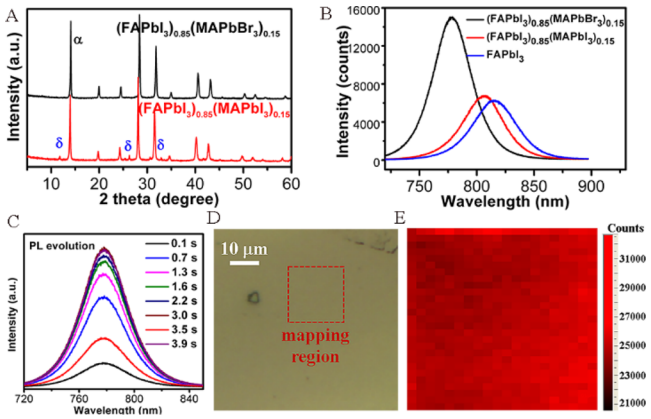

Figure 5. (A) XRD pattern of alloyed perovskite single crystals of $x = 0.15$ with and without Br incorporation; (B) steady-state PL intensity of $FAPbI_3$-based perovskites (red: multiply by 5); (C) light soaking effect for $x = 0.15$; (D) optical morphology; (E) PL mapping of the $x = 0.15$ crystal surface in 20 × 20 μm.

even stronger than that of $(FAPbI_3)_{0.95}(MAPbBr_3)_{0.05}$, shown in Figure 3A. This demonstrates that Br indeed plays important roles in phase stabilization of the mixed perovskite even at very low ratio. Considering the fact that the rate of α-to-δ phase transition in $FAPbI_3$ depends on the crystal quality of the $FAPbI_3$ (see details in Figure S7), the role of Br incorporation may lie in crystal growth with better quality. To prove the hypothesis, the steady-state PL was measured on a spatially resolved confocal microscope. The PL intensity increases dramatically when bromide is incorporated compared to $FAPbI_3$ and $(FAPbI_3)_{0.85}(MAPbI_3)_{0.15}$, as can be seen in Figure 5B. This indicates Br plays a crucial role in suppressing nonradiative recombination. The carrier lifetime of this perovskite reaches 11.0 μs, which is over 20 times of that of $FAPbI_3$ (Figure S8 and S9). Besides, the PL evolution[30] quickly reaches to a maximum within 3.5 s, which implies low defects density in $(FAPbI_3)_{0.85}(MAPbBr_3)_{0.15}$. These improved optical properties confirm the promotion of crystal quality of the MA^+ and Br^- incorporated perovskite. On the other hand, the spatially resolved PL mapping demonstrates a uniform surface in terms of intensity fluctuation within the limit of spatial resolution of 1 × 1 μm, as shown in Figure 5D,E, which suggests the reduction of defect density is not caused by surface passivation in Br-based perovskite.

The improved crystal quality of the Br-incorporated perovskite, distinctive with reduced defect density, discloses the role of Br in crystallization kinetics of the mixed perovskite. Interestingly, though the solubility of $MAPbBr_3$ perovskite alone (or $PbBr_2$+MABr precursors) in GBL is reported to be less than 0.05 mg/mL (~0.1 mol/L) at room temperature or 80 °C due to weak interaction between the solute and GBL,[25] we can obtain uniform and clear solution of mixed cations and halides perovskites of $(FAPbI_3)_{1-x}(MAPbBr_3)_x$ in the case of $x = 0.15$ (0.15 mol/L $PbBr_2$+MABr) and even $x = 0.20$ (0.20 mol/L $PbBr_2$+MABr). The increased solubility (see Figure S10) of the bromide precursors is most likely due to the halide exchange process of and Br^- with I^- during dissolution.[31,32] We observed the preferential dissolution of PbI_2 and FAI to form a yellow upper solution after 2 h without stirring while the red Br-terminated perovskites solid was left at the bottom of the container, the latter being slowly dissolved after at least another 12 h. When the clear precursor solution is heated to 100 °C, the Br-terminated perovskite species are expected to nucleate first due to its low solubility in GBL. This nucleation process is supported by the observation of dramatically enhanced crystal growth rate upon increase of concentration of Br-based precursors. The approximate time to obtain visible black perovskite crystals is illustrated in Figure S11. We also note that it is difficult to harvest large crystals when x increases to 0.20, because the nucleation process occurs so fast that too many small crystals will form, which hinders their further growth into large crystals (see optical photograph in Figure S1). These observations confirm the Br-induced crystallization process. It is deserved to be mentioned that $MAPbBr_3$ adapts cubic phase symmetry and exhibits lower surface energy[33] so that the Br-induced crystallization may result in a better crystallization of cubic perovskite phase with significantly reduced defect density, thus hindering the formation of the yellow nonperovskite phase.

It has been shown that both cations and halides are important to stabilize the perovskite phase. Specially, the nucleation of Br-based perovskite is crucial, which can induce a better crystal quality with low defect density. This guides us to fabricate perovskite solar cells using the $(FAPbI_3)_{0.85}(MAPbBr_3)_{0.15}$ films. Because of the difficulties in kinetic control of faster crystallization during spin-coating, it seems unlikely to obtain red Br-terminated-perovskite-rich films with large grain size using one-step method (see Figure S12). The interplay between precursors and solvents becomes highly important in spin-coating process and serves as an additional factor to be managed for the preparation of mixed perovskites. We demonstrate that the desired film composition and morphology can be achieved simultaneously by using optimized amount of DMSO as a cosolvent with DMF to slow down slightly the initial nucleation of $MAPbBr_3$. We can acquire a champion $(FAPbI_3)_{0.85}(MAPbBr_3)_{0.15}$ perovskite solar cell with average PCE of 19.5% (see Figure S13 and detailed cell performance characterization in Figure S14 and S15), whereas the $x = 0.05$ perovskite

DOI: 10.1021/jacs.6b12432
J. Am. Chem. Soc. 2017, 139, 3320−3323

with insufficient δ-phase inhibition exhibits much lower average PCE of 12.1% and enormous hysteresis.

In conclusion, by growing and employing high-quality mixed cations and halides perovskite single crystals with extremely long carrier lifetime, we have investigated the thermodynamic and kinetic effect of MA^+ and Br^- incorporation on cubic phase stabilization of FA-based perovskite. The incorporation of MA^+ stabilizes the cubic phase perovskite through contracting the lattice, increasing the cation disorder and thus lowering the Gibbs free energy; whereas the incorporation of Br^- changes the crystallization kinetics by accommodating the difference in the precursor−solvent interaction strength for bromide- and iodine-based species. These findings advance the understanding on the underlying mechanism of cubic phase stabilization behavior of the highly important mixed cations and halides perovskite system in solar cells, and may shed light on the design and fabrication of high-performance FA-based perovskite solar cells with better phase stability.

■ ASSOCIATED CONTENT

Supporting Information

The Supporting Information is available free of charge on the ACS Publications website at DOI: 10.1021/jacs.6b12432.

Full experimental details and additional characterizations (PDF)

Crystal structure file of $(FAPbI_3)_{0.85}(MAPbBr_3)_{0.15}$ (CIF)

■ AUTHOR INFORMATION

Corresponding Author

*bwmao@xmu.edu.cn

ORCID

Bing-Wei Mao: 0000-0002-9015-0162

Zhong-Qun Tian: 0000-0002-9775-8189

Author Contributions

†These authors contributed equally.

Notes

The authors declare no competing financial interest.

■ ACKNOWLEDGMENTS

We acknowledge the supports of MOST (Grant 2016YFA0200703) and NSFC (21473147, 21321062).

■ REFERENCES

(1) Kojima, A.; Teshima, K.; Shirai, Y.; Miyasaka, T. *J. Am. Chem. Soc.* **2009**, *131*, 6050.

(2) Kim, H. S.; Lee, C. R.; Im, J. H.; Lee, K. B.; Moehl, T.; Marchioro, A.; Moon, S. J.; Humphry-Baker, R.; Yum, J. H.; Moser, J. E.; Gratzel, M.; Park, N. G. *Sci. Rep.* **2012**, *2*, 591.

(3) Burschka, J.; Pellet, N.; Moon, S. J.; Humphry-Baker, R.; Gao, P.; Nazeeruddin, M. K.; Gratzel, M. *Nature* **2013**, *499*, 316.

(4) Liu, M. Z.; Johnston, M. B.; Snaith, H. J. *Nature* **2013**, *501*, 395.

(5) Chen, W.; Wu, Y.; Yue, Y.; Liu, J.; Zhang, W.; Yang, X.; Chen, H.; Bi, E.; Ashraful, I.; Grätzel, M.; Han, L. *Science* **2015**, *350*, 944.

(6) McMeekin, D. P.; Sadoughi, G.; Rehman, W.; Eperon, G. E.; Saliba, M.; Hörantner, M. T.; Haghighirad, A.; Sakai, N.; Korte, L.; Rech, B.; Johnston, M. B.; Herz, L. M.; Snaith, H. J. *Science* **2016**, *351*, 151.

(7) NREL. Research Cell Efficiency Records. www.nrel.gov/ncpv/images/efficiency_chart.jpg.

(8) Jeon, N. J.; Noh, J. H.; Yang, W. S.; Kim, Y. C.; Ryu, S.; Seo, J.; Seok, S. I. *Nature* **2015**, *517*, 476.

(9) Pellet, N.; Gao, P.; Gregori, G.; Yang, T. Y.; Nazeeruddin, M. K.; Maier, J.; Gratzel, M. *Angew. Chem., Int. Ed.* **2014**, *53*, 3151.

(10) Fang, Y.; Dong, Q.; Shao, Y.; Yuan, Y.; Huang, J. *Nat. Photonics* **2015**, *9*, 679.

(11) Eperon, G. E.; Leijtens, T.; Bush, K. A.; Prasanna, R.; Green, T.; Wang, J. T.-W.; McMeekin, D. P.; Volonakis, G.; Milot, R. L.; May, R.; Palmstrom, A.; Slotcavage, D. J.; Belisle, R. A.; Patel, J. B.; Parrott, E. S.; Sutton, R. J.; Ma, W.; Moghadam, F.; Conings, B.; Babayigit, A.; Boyen, H. G.; Bent, S.; Giustino, F.; Herz, L. M.; Johnston, M. B.; McGehee, M. D.; Snaith, H. J. *Science* **2016**, *354*, 861.

(12) Liu, Y.; Yang, Z.; Cui, D.; Ren, X.; Sun, J.; Liu, X.; Zhang, J.; Wei, Q.; Fan, H.; Yu, F.; Zhang, X.; Zhao, C.; Liu, S. *Adv. Mater.* **2015**, *27*, 5176.

(13) Zhumekenov, A. A.; Saidaminov, M. I.; Haque, M. A.; Alarousu, E.; Sarmah, S. P.; Murali, B.; Dursun, I.; Miao, X.-H.; Abdelhady, A. L.; Wu, T.; Mohammed, O. F.; Bakr, O. M. *ACS Energy Lett.* **2016**, *1*, 32.

(14) Yang, W. S.; Noh, J. H.; Jeon, N. J.; Kim, Y. C.; Ryu, S.; Seo, J.; Seok, S. I. *Science* **2015**, *348*, 1234.

(15) Liu, Y.; Sun, J.; Yang, Z.; Yang, D.; Ren, X.; Xu, H.; Yang, Z.; Liu, S. *Adv. Opt. Mater.* **2016**, *4*, 1829−1837.

(16) Lee, J.-W.; Kim, D.-H.; Kim, H.-S.; Seo, S.-W.; Cho, S. M.; Park, N.-G. *Adv. Energy. Mater.* **2015**, 5.

(17) Yi, C.; Luo, J.; Meloni, S.; Boziki, A.; Ashari-Astani, N.; Gratzel, C.; Zakeeruddin, S. M.; Rothlisberger, U.; Gratzel, M. *Energy Environ. Sci.* **2016**, *9*, 656.

(18) Saliba, M.; Matsui, T.; Domanski, K.; Seo, J.-Y.; Ummadisingu, A.; Zakeeruddin, S. M.; Correa-Baena, J.-P.; Tress, W. R.; Abate, A.; Hagfeldt, A.; Grätzel, M. *Science* **2016**, *354*, 206.

(19) Saliba, M.; Matsui, T.; Seo, J.-Y.; Domanski, K.; Correa-Baena, J.-P.; Nazeeruddin, M. K.; Zakeeruddin, S. M.; Tress, W.; Abate, A.; Hagfeldt, A.; Gratzel, M. *Energy Environ. Sci.* **2016**, *9*, 1989−1997.

(20) Li, Z.; Yang, M.; Park, J.-S.; Wei, S.-H.; Berry, J. J.; Zhu, K. *Chem. Mater.* **2016**, *28*, 284.

(21) Zheng, X.; Wu, C.; Jha, S. K.; Li, Z.; Zhu, K.; Priya, S. *ACS Energy Lett.* **2016**, *1*, 1014.

(22) Chen, T.; Foley, B. J.; Park, C.; Brown, C. M.; Harriger, L. W.; Lee, J.; Ruff, J.; Yoon, M.; Choi, J. J.; Lee, S.-H. *Sci. Adv.* **2016**, *2*, e1601650.

(23) Xiao, M.; Huang, F.; Huang, W.; Dkhissi, Y.; Zhu, Y.; Etheridge, J.; Gray-Weale, A.; Bach, U.; Cheng, Y.-B.; Spiccia, L. *Angew. Chem., Int. Ed.* **2014**, *53*, 9898.

(24) Han, Q.; Bae, S.-H.; Sun, P.; Hsieh, Y.-T.; Yang, Y.; Rim, Y. S.; Zhao, H.; Chen, Q.; Shi, W.; Li, G.; Yang, Y. *Adv. Mater.* **2016**, *28*, 2253.

(25) Saidaminov, M. I.; Abdelhady, A. L.; Murali, B.; Alarousu, E.; Burlakov, V. M.; Peng, W.; Dursun, I.; Wang, L.; He, Y.; Maculan, G.; Goriely, A.; Wu, T.; Mohammed, O. F.; Bakr, O. M. *Nat. Commun.* **2015**, *6*, 7586.

(26) Zhang, T.; Yang, M.; Benson, E. E.; Li, Z.; van de Lagemaat, J.; Luther, J. M.; Yan, Y.; Zhu, K.; Zhao, Y. *Chem. Commun.* **2015**, *51*, 7820.

(27) Weller, M. T.; Weber, O. J.; Frost, J. M.; Walsh, A. *J. Phys. Chem. Lett.* **2015**, *6*, 3209.

(28) Kieslich, G.; Sun, S.; Cheetham, A. K. *Chem. Sci.* **2014**, *5*, 4712.

(29) Weller, M. T.; Weber, O. J.; Charles, B. *J. Mater. Chem. A* **2016**, *4*, 15375−15382.

(30) Fang, H.-H.; Wang, F.; Adjokatse, S.; Zhao, N.; Loi, M. A. *Adv. Funct. Mater.* **2016**, *26*, 4653.

(31) Zhou, Y.; Yang, M.; Pang, S.; Zhu, K.; Padture, N. P. *J. Am. Chem. Soc.* **2016**, *138*, 5535.

(32) Ibrahim Dar, M.; Abdi-Jalebi, M.; Arora, N.; Moehl, T.; Gratzel, M.; Nazeeruddin, M. K. *Adv. Mater.* **2015**, *27*, 7221.

(33) Yang, M.; Zhang, T.; Schulz, P.; Li, Z.; Li, G.; Kim, D. H.; Guo, N.; Berry, J. J.; Zhu, K.; Zhao, Y. *Nat. Commun.* **2016**, *7*, 12305.

DOI: 10.1021/jacs.6b12432
J. Am. Chem. Soc. 2017, 139, 3320−3323